

# Enhancing Fault Detection and Isolation in an All-Electric Auxiliary Power Unit (APU) Gas Generator by Utilizing Starter/Generator Signal

Haotian Mao, Khashayar Khorasani, and Yingqing Guo

**Abstract**—This study proposes a novel paradigm for enhancing fault detection and isolation (FDI) of gas generators in all-electric auxiliary power unit (APU) by utilizing shaft power information from the starter/generator. First, we conduct a pioneering investigation into the challenges and opportunities for FDI brought about by APU electrification. Our analysis reveals that the electrification of APU opens up new possibilities for utilizing shaft power estimates from starter/generator to improve gas generator FDI. We then provide comprehensive theoretical and analytical evidence demonstrating why, how, and to what extent, the shaft power information from the starter/generator can fundamentally enhance the estimation accuracy of system states and health parameters of the gas generator, while also identifying the key factors influencing these improvements in FDI performance. The effectiveness of the proposed paradigm and its theoretical foundations are validated through extensive Monte Carlo simulations. Furthermore, through comprehensive comparative analysis with state-of-the-art gas generator fault diagnosis methods, our experimental results not only demonstrate the superior performance of the proposed approach but also validate that the diagnostic capabilities of existing advanced FDI techniques can be substantially enhanced by incorporating shaft power information. And the observed performance improvement patterns strongly align with our theoretical analysis, verifying both the effectiveness and guiding significance of our theoretical framework. These research findings provide a unique perspective in answering three fundamental questions: why joint fault diagnosis of the starter/generator and gas generator is essential, how it can be implemented, and what factors determine its effectiveness, thereby opening up promising new avenues for FDI technologies in all-electric APU systems.

**Index Terms**—Auxiliary power unit (APU), all-electric, starter/generator, gas generator, Bayesian estimation, fault detection and isolation (FDI).

## I. INTRODUCTION

To address the escalating need for air travel and its imminent economic and environmental ramifications, the most viable solution at present is the aircraft electrification. While the notion of an all-electric aircraft (AEA) remains unrealized, the concept of more electric aircraft (MEA) has elicited considerable interest. In these systems, electrical counterparts supplement or entirely supplant the cumbersome, inefficient hydraulic and pneumatic systems that are characteristic of conventional aircraft [1, 2]. Due to this trend, the functionality and structure of the auxiliary power unit (APU) have undergone significant changes, transitioning from the conventional APU that provided

aerodynamic, hydraulic, and electrical power to an all-electric APU that solely provides electrical power [3, 4].

The all-electric APU has been implemented on the Boeing 787 aircraft. The key difference between the traditional APU and the all-electric APU is that the latter is equipped with a high-power electric starter/generator and eliminates the pneumatic and hydraulic functions and their associated components of the APU [3].

The estimation and diagnosis of APU failures are critically important for flight safety, as the APU is closely related to the key energy supply of the aircraft and serves as a vital component for starting the main engines. Additionally, estimating degradation and health conditions are beneficial for achieving condition-based maintenance (CBM), which can reduce maintenance cost. Consequently, numerous studies have been conducted on APU failure and health condition estimation, including those focused on gas generators and starter/generators [5-12].

The authors in [7] proposed a method for identifying the health status of gas generator components based on the recognition of system performance parameters. This method trains a classification algorithm for each system component to identify its health status. As compared to the training strategy based on a single fault assumption, the training strategy considering multiple component faults provides more accurate diagnostic estimation. The authors in [8] proposed a method that combines long short-term memory (LSTM) network and support vector regression (SVR) techniques with a Kalman filter to estimate key performance parameters of gas generators. The authors in [9] utilized the random forest method to establish a performance baseline model for APU, and then obtained estimates of health indices characterizing the performance degradation of the in-service APU based on the performance baseline model. The authors in [13] proposed a multi-time window convolutional bidirectional long short-term memory neural network for FDI of APU in civil aircraft.

The authors in [10] presented the time-to-failure analysis on more-electric aircraft starter/generator relying on the physics of failure approach, with a special focus on turn-to-turn short-circuit faults. The authors in [11] utilized the extended Kalman filter (EKF) to estimate inter-turn short circuit faults in the APU aircraft starter/generator. The authors in [12] proposed a method based on stacked autoencoders (SAE) and support vector data description (SVDD) for detecting rectifier faults in the aircraft starter/generator.

However, the above studies have been conducted focusing on individual components, such as gas generator or

Haotian Mao and Yingqing Guo are with the School of Power and Energy, Northwestern Polytechnical University, Xi'an 710072, China (email: alexmao@mail.nwpu.edu.cn; yqguo@nwpu.edu.cn). Haotian Mao would like to also acknowledge the partial support that he has received from the China Scholarship Council under Grant 201906290241.

Khashayar Khorasani is with the Department of Electrical and Computer Engineering, Concordia University, Montreal, QC H3G 1M8, Canada (e-mail: kash@ece.concordia.ca).

starter/generator. This approach of conducting fault estimation research on each component separately is feasible in the traditional APU. Nevertheless, for the all-electric APU, this isolated approach is not the optimal solution, due to strong coupling relationship between starter/generator and gas generator of an all-electric APU. On one hand, this coupling causes malfunction of either component to severely affect the operation of the other, posing a challenge to our fault estimation results. On the other hand, one can utilize this coupling relationship to introduce new external information into the fault estimation of individual components, thereby enhancing the fault estimation capability, which presents opportunities for improving the fault estimation results. This paper will conduct an in-depth investigation into this opportunity, exploring the enhancement of our capability in estimating gas generator faults through utilization of starter/generator signals.

The organization of this paper is as follows. Section II, introduces our research objectives, the all-electric APU, and conduct an in-depth analysis of the opportunities and challenges in fault diagnosis that are brought by the electrification of APU. Section III, provides the premises and assumptions for our proposed methodology. Section IV, presents the posterior estimates using and not using the shaft power estimate from the starter/generator. Section V, explores the differences in estimation accuracy between the two estimates, aiming to demonstrate how the information of shaft power from the starter/generator can improve the accuracy of the gas generator fault estimation and identifies factors that affect the magnitude of this improvement. Section VI, presents the Monte Carlo simulation results, validating the improvement in estimation accuracy that is achieved through incorporating the shaft power data from the starter/generator. Additionally, it demonstrates that employing a more accurate model or estimating additional health parameters can significantly enhance the utility of the shaft power information on fault estimation, as well as in Fault Detection and Isolation (FDI) objectives.

## II. STATE OF PROBLEM AND RESEARCH OBJECTIVES

In this section, we will first introduce an all-electric APU and then present our analysis of the opportunities and challenges that the electrification of the APU brings about to fault estimation problem. Finally, we will briefly outline the research objectives of our study.

Our research focuses on an all-electric APU, primarily comprising a gas generator and a high-power starter/generator. The gas generator operates as a turboshaft, producing minimal thrust while primarily generating power via its output shaft [14]. The starter/generator, on the other hand, functions as a brushless wound-field synchronous generator (BWFSG) [15]. The operational mechanism of an all-electric APU involves the gas generator transmitting power to the starter/generator via the drive shaft, thereby enabling the starter/generator to generate electricity and supply power to the aircraft [16].

The all-electric APU is an evolution from the traditional APU. Conventionally, aircraft requires the APU to supply electrical, pneumatic, and hydraulic energy. Therefore, the shaft power output of the traditional APU is required to drive the starter/generator for electrical energy, the compressor for pneumatic energy, and the equipment for hydraulic energy.

However, with the electrification of aircraft, the more electric aircraft no longer requires the APU to provide pneumatic and hydraulic energy, but only the electrical energy from the APU. This implies that the all-electric APU, as opposed to the traditional APU, only needs the shaft power to drive a high-power starter/generator.

The principles and structures of traditional APU and the all-electric APU is in the form that are shown in Fig. 1. The dashed line represents the components that are reduced in an all-electric APU as compared to the traditional APU. It can be seen that the all-electric APU eliminates two components that convert rotational power into pneumatic and hydraulic energy, resulting in a simpler structure. This brings about both opportunities and challenges for fault estimation in the APU.

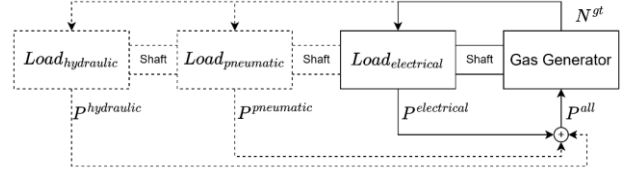


**Fig. 1.** Comparison between the traditional APU and an all-electric APU.

On one hand, this establishes a strong coupling relationship between the starter/generator and the gas generator, causing their faults to have significant impacts on each other and rendering starter/generator faults more critical [7, 17]. This presents a new challenge for our FDI approach. On the other hand, it also offers opportunities to leverage this relationship to enhance our FDI methodology and performance. By utilizing information from one system, one can improve the estimates of the other system. This paper will focus on this opportunity and specifically illustrate how information from the starter/generator can be used to enhance the FDI performance of the gas generator.

Given that the energy output of a gas generator in an all-electric APU is solely reserved for the electrical part of the generator, an opportunity arises for us to precisely estimate the power output (shaft power) of the gas generator, thereby improving the accuracy of the fault diagnosis scheme in the gas generator.

The energy output of a traditional APU gas generator equals the sum of the energy consumed by the starter/generator that supplies electrical energy to the aircraft, the compressor that supplies the pneumatic energy, and the hydraulic pump that supplies the hydraulic energy. As a component of the electrical system, the power consumed by the starter/generator can be estimated through measurable electrical measurements. However, the energy consumed by compressor and hydraulic pump is influenced by numerous factors, and obtaining accurate relevant parameters is a highly challenging task. Therefore, making a precise estimate of their power consumption is quite challenging. Moreover, due to the compact structure of the APU, installing torque or power sensors inside it poses significant challenges, that has always made estimating the power of the gas generator a complex task [18, 19].

The advent of an all-electric APU offers a solution to the above problem. Without the compressor and hydraulic pump, one can estimate the power of starter/generator with relative

> REPLACE THIS LINE WITH YOUR MANUSCRIPT ID NUMBER (DOUBLE-CLICK HERE TO EDIT) <

precision, thereby obtaining a fairly accurate estimate of power output of the gas generator. This information on the shaft power of gas generator can significantly enhance estimation accuracy of states and health parameters of gas generator.

The feasibility of the above concept has already been demonstrated in other similar electro-mechanical systems, such as the hybrid electric vehicle and wind power generation industries. The range-extended electric vehicle (REEV) is an electric car powered by a battery and equipped with an on-board range extender generator, also known as an auxiliary power unit (REEV-APU). When the battery charge level is low, the range extender automatically starts and charges the battery. The REEV-APU consists of an engine and a generator, where the engine is solely responsible for driving the generator, which in turn supplies electrical power to the vehicle. Researchers in this field have conducted extensive studies on how to utilize the generator to estimate engine's shaft power, and utilize power estimation to improve parameter estimation and performance of REEV-APU [20-22]. Similarly, the wind power generation system primarily comprises a generator and a mechanical wind turbine, where the wind turbine, driven by wind power, serves as the prime mover that drives the generator to produce electricity. Researchers in this field have also conducted a substantial amount of research on how to utilize the generator's signals, including shaft power information, to estimate the parameters, monitor the conditions, and diagnose faults of the wind turbine [23, 24].

In this study, our aim and objective are to investigate why, how and to what extent shaft power estimates from the starter/generator can enhance system state and health parameter estimation in an all-electric APU gas generator, thereby improving FDI performance.

### III. PRELIMINARIES

In this section, we introduce the gas generator model that is employed in our study and describe its characteristics. We will then introduce the methodological framework that is adopted to carry out our research.

#### A. Gas Generator Model

We assume that the dynamics of the gas generator can be modeled by a linear system, that is expressed in the following state-space representation [25, 26],

$$\begin{aligned} x(t_{k+1}) &= A(t_k)x(t_k) + B(t_k)u(t_k) + E(t_k)\theta(t_k) \\ &\quad + F(t_k)Pe(t_k) + w(t_k) \\ y(t_k) &= C(t_k)x(t_k) + D(t_k)u(t_k) \\ &\quad + G(t_k)\theta(t_k) + v(t_k) \end{aligned} \quad (1)$$

where  $u$  represents the gas generator input,  $y$  represents the measurements,  $\theta$  denotes the health parameters that represent gas generator faults or degradation,  $Pe$  represents the shaft power,  $x$  represents the state variables,  $A$ ,  $B$ ,  $C$ ,  $D$ ,  $E$ ,  $F$ ,  $G$  represent the known matrices of the state-space model corresponding to the system, and  $w$ ,  $v$  represent two independent Gaussian white noise processes with zero mean, corresponding to process and measurement noise, respectively.

In the context of a gas turbine system, it is a reasonable assumption that the power output from the shaft affects all rotor

speeds and state parameters. Each measurement is influenced by at least one state variable, and each health parameter impacts at least one measurement. To formalize these assumptions, it can be noted that all elements in the column vector  $F$  are non-zero. Moreover, the matrix  $C$  does not contain any rows composed entirely of zero elements, and the matrix  $G$  does not have any columns composed entirely of zero elements.

Furthermore, given the operational characteristics of an all-electric APU, it is hypothesized that the health parameters demonstrate gradual evolutionary patterns, with their specific degradation trajectories being inherently uncertain a priori. Simultaneously, the shaft power, predominantly determined by electrical loading conditions, is subject to substantial stochastic variations and may undergo rapid transient changes [27, 28]. Within this framework, it is assumed that the starter/generator system provides high-fidelity shaft power estimates and associated covariance matrices at each temporal increment, with these estimates conforming to a Gaussian probability distribution. This assumption allows us to abstract away from the technical complexities of obtaining precise shaft power estimates, such as noise mitigation strategies and signal loss compensation mechanisms, thereby maintaining the investigative focus on the fundamental relationship between shaft power estimation and gas generator fault diagnosis and isolation (FDI) capabilities.

**Remark 1:** The linear system representation, along with typical all-electric APU characteristics assumptions, is adopted in this work for two reasons. First, it enables a generalized analysis of shaft power information's impact on the FDI scheme, rather than focusing on specific APU structures. Second, the gas generator's slow and relatively linear dynamic response makes linear/piecewise linear approximation a valid approach, which has been widely adopted in relevant literature [29-32].

#### B. Proposed Methodology

The premise of a linear system allows the application of linear state estimation techniques to estimate system states, health parameters, and to assess the influence of shaft power estimates, that are obtained from the starter/generator.

This study introduces two estimates: the posterior estimates with no shaft power information (PENS) and the posterior estimates with shaft power information (PES). We will demonstrate that the PENS represent the posterior estimates of health parameters and system states in absence of accurate shaft power estimates at each step. Conversely, the PES represents the posterior estimates of these variables when accurate shaft power estimates, derived from the starter/generator, are available at each step.

Comparing the accuracy of the PES and PENS allows one to assess the impact of shaft power estimates from starter/generator on these estimates. By analyzing this impact, one can determine how the shaft power estimates derived from the starter/generator can enhance the FDI in gas generators and identify factors that affect the magnitude of this enhancement. Finally, we employ Monte Carlo simulations to validate our proposed methodology and to analyze how the significance of shaft power information changes in response to variations in the accuracy of the model that is used for the estimation and the number of health parameters.

> REPLACE THIS LINE WITH YOUR MANUSCRIPT ID NUMBER (DOUBLE-CLICK HERE TO EDIT) <

#### IV. TWO POSTERIOR ESTIMATES: WITH AND WITHOUT SHAFT POWER INFORMATION FROM STARTER/GENERATOR SIGNALS

In this section, we introduce two different estimation scenarios. The first scenario involves estimating system states and health parameters with the aid of an accurate shaft power estimate from the starter/generator. The second scenario proceeds without such information. For these two scenarios, we then define two corresponding posterior estimates: the posterior estimates with shaft power information (PES) and the posterior estimate with no shaft power information (PENS). Subsequently, we propose two algorithms specifically designed to compute and derive these two estimates.

##### A. Definition of Two Scenarios and Two Posterior Estimates

Considering the system that is described by equation (1), we assume a given Gaussian distribution for the initial system states  $x(t_0)$  and health parameters  $\theta(t_0)$ . The inputs  $u(t_k)$  and measurements  $y(t_k)$  are also available for each time step. The posterior estimates of the health parameters at the time step  $t_{k-1}$ , denoted by  $\hat{\theta}(t_{k-1})$ , are utilized to compute the prior estimate  $\tilde{\theta}(t_k)$ , at the subsequent time step  $t_k$ , that is expressed as  $\tilde{\theta}(t_k) = \hat{\theta}(t_{k-1}) + w^h(t_k)$ , where  $w^h(t_k)$  represents noise that accounts for the uncertainty in the health parameters due to the underlying slowly degradation process.

*Scenario 1 (PES):* A given Gaussian estimate  $Pe$  and the corresponding covariance  $P^{Pe}$  for the shaft power from the starter/generator is available at each time step. The PES is defined as posterior estimates of system states and health parameters at each time step given the conditions outlined above.

*Scenario 2 (PENS):* The pre-set values  $PeT$  and  $P^{PeT}$  are utilized as the estimated value and the covariance of the shaft power for each time step, where  $PeT$  represents the shaft power value under a typical operating condition and  $P^{PeT}$  is a sufficiently large value. The PENS is defined as posterior estimates of system states, health parameters at each time step given conditions outlined above.

The health parameters, as assumed above, change slowly. Thus, the value at the next time step is almost the same as that of the previous one. Consequently, we choose to use the posterior estimate from the last time step and noise to derive the prior estimate for the next time step in both scenarios [25, 26]. Due to absence of shaft power data in Scenario 2, we selected  $PeT$  and  $P^{PeT}$  as estimation values and covariances of the shaft power to address the uncertainty associated with the shaft power, aiming for accurate posterior estimates.

**Remark 2:** The above two estimation scenarios, for the first time, clearly define the estimation process and the achievable posterior estimates under two conditions: with/without shaft power information. This novel framework enables the evaluation of shaft power information's influence through comparative analysis of estimation accuracy and FDI performance between PES and PENS.

##### B. Algorithms for the Two Posterior Estimates

According to the characteristics of the gas generator and the definition of Scenario 1, one can incorporate health parameters into the system states, as outlined in equation (2), to obtain the PES [25, 26], that is

$$\begin{aligned} x^{aug}(t_{k+1}) &= A^{aug}(t_k)x^{aug}(t_k) + B^{aug}(t_k)u(t_k) \\ &\quad + F^{aug}(t_k)Pe(t_k) + w^{aug}(t_k) \\ y(t_k) &= C^{aug}(t_k)x^{aug}(t_k) + D(t_k)u(t_k) + v(t_k) \end{aligned} \quad (2)$$

where

$$\begin{aligned} A^{aug}(t_k) &= \begin{bmatrix} A(t_k) & E(t_k) \\ 0 & I \end{bmatrix}, B^{aug}(t_k) = \begin{bmatrix} B(t_k) \\ 0 \end{bmatrix}, \\ C^{aug}(t_k) &= [C(t_k) \quad G(t_k)], F^{aug}(t_k) = \begin{bmatrix} F(t_k) \\ 0 \end{bmatrix}, \\ Q^{aug} &= E[w^{aug}(t_k)w^{aug}(t_k)^T], R = E[v(t_k)v(t_k)^T], \\ w^{aug}(t_k) &= \begin{bmatrix} w(t_k) & 0 \\ 0 & w^h(t_k) \end{bmatrix}, x^{gr} = \begin{bmatrix} x^{gr} \\ \theta^{gr} \end{bmatrix}, \end{aligned}$$

and the superscript *aug* denotes the augmented variable.

Following the above augmentation, state estimation scheme can be utilized to achieve the PES. By definition of Scenario 1 and equation (2), the prior estimates and covariance update process for achieving PES can be described by:

$$\begin{aligned} \tilde{x}^{aug}(t_k) &= A^{aug}(t_k)\hat{x}^{aug}(t_{k-1}) + B^{aug}(t_k)u(t_k) \\ &\quad + F^{aug}(t_k)Pe(t_k) \end{aligned} \quad (3)$$

$$\begin{aligned} \tilde{P}^{aug}(t_k) &= A^{aug}(t_k)\hat{P}^{aug}(t_{k-1})A^{aug}(t_k)^T \\ &\quad + F^{aug}(t_k)P^{Pe}(t_k)F^{aug}(t_k)^T + Q^{aug}(t_k) \end{aligned} \quad (4)$$

where the superscript  $\sim$  represents parameters related to prior estimate and  $\tilde{P}^{aug}$  represents covariance of the prior estimate.

When we have the above prior estimates and covariance, one can employ Kalman filter theory to obtain the PES. The corresponding Kalman gain update equation, posterior estimate and the covariance update equations for achieving the PES can be expressed by [33]:

$$\begin{aligned} K^{aug}(t_k) &= \tilde{P}^{aug}(t_k)C^{aug}(t_k)^T \\ &\quad (C^{aug}(t_k)\tilde{P}^{aug}(t_k)C^{aug}(t_k)^T + R(t_k))^{-1} \end{aligned} \quad (5)$$

$$\begin{aligned} \hat{x}^{aug}(t_k) &= \tilde{x}^{aug}(t_k) + K^{aug}(t_k) \\ &\quad (y(t_k) - C^{aug}\tilde{x}^{aug}(t_k) - D(t_k)u(t_k)) \end{aligned} \quad (6)$$

$$\begin{aligned} \hat{P}^{aug}(t_k) &= (I - K^{aug}(t_k)C^{aug}(t_k))\tilde{P}^{aug}(t_k) \\ &\quad (I - K^{aug}(t_k)C^{aug}(t_k))^T + K^{aug}(t_k)R(t_k)K^{aug}(t_k)^T \end{aligned} \quad (7)$$

where the superscript  $\hat{\cdot}$  represents the parameters related to the posterior estimate,  $\hat{P}^{aug}$  denotes the posterior estimate covariance matrix, and  $K^{aug}$  represents the Kalman gain.

By combining the above prior and posterior update equations (3)-(7), Algorithm 1 can be derived for obtaining the PES as shown in Fig. 2.

To obtain the PENS, it is also practical to incorporate health parameters and shaft power into the system states, as demonstrated in equation (2).

By definition of Scenario 2, the prior estimates and the covariance update process for achieving the PENS can be described by:

> REPLACE THIS LINE WITH YOUR MANUSCRIPT ID NUMBER (DOUBLE-CLICK HERE TO EDIT) <

$$\tilde{x}^{aug}(t_k) = A^{aug}(t_k)\hat{x}^{aug}(t_{k-1}) + B^{aug}(t_k)u^{aug}(t_k) + F^{aug}(t_k)PeT(t_k) \quad (8)$$

$$\tilde{P}^{aug}(t_k) = A^{aug}(t_k)\hat{P}^{gt}(t_{k-1})A^{aug}(t_k)^T + F^{aug}(t_k)P^{PeT}(t_k)F^{aug}(t_k)^T + Q^{aug}(t_k) \quad (9)$$

The corresponding Kalman gain update equation, posterior estimate and the covariance update equation for achieving the PENS can also be expressed by equation (5)-(7) above.

---

**Algorithm 1:** Posterior estimates with shaft power information (PES)

---

**Input :** Engine augmented state space matrix:  
 $A^{aug}(t_{k-1}), B^{aug}(t_{k-1}), C^{aug}(t_k), D^{aug}(t_k), F^{aug}(t_{k-1});$   
 Posterior state estimate and covariance at  $t_{k-1}$ :  
 $\hat{x}^{aug}(t_{k-1}), \hat{P}^{aug}(t_{k-1});$   
 Shaft power estimate from starter/generator and corresponding covariance:  
 $Pe(t_k), P^{Pe}(t_k);$

**Output:** Posterior state estimate and covariance at  $t_k$ :  
 $\hat{x}^{aug}(t_k), \hat{P}^{aug}(t_k);$

**Step 1 : Predict**

1. Predict the prior estimate  $\tilde{x}^{aug}(t_k)$  based on Equation (3);
2. Predict the prior estimate covariance  $\tilde{P}^{aug}(t_k)$  based on Equation (4);

**Step 2 : Update**

1. Obtain the Kalman gain  $K^{aug}(t_k)$  based on Equation (5);
  2. Update posterior state estimate  $\hat{x}^{aug}(t_k)$  based on Equation (6);
  3. Update posterior state estimate covariance  $\hat{P}^{aug}(t_k)$  based on Equation (7);
- 

Fig. 2. Algorithm 1 for the PENS.

By combining the prior equations (8), (9) and posterior equations (5)-(7), the Algorithm 2 can be derived to obtain the PENS as follows:

---

**Algorithm 2:** Posterior estimates with no shaft power information (PENS)

---

**Input :** Engine augmented state space matrix:  
 $A^{aug}(t_{k-1}), B^{aug}(t_{k-1}), C^{aug}(t_k), D^{aug}(t_k), F^{aug}(t_k);$   
 Posterior state estimate and covariance at  $t_{k-1}$ :  
 $\hat{x}^{aug}(t_{k-1}), \hat{P}^{aug}(t_{k-1});$

**Output:** Posterior state estimate and covariance at  $t_k$ :  
 $\hat{x}^{aug}(t_k), \hat{P}^{aug}(t_k);$

**Step 1 : Predict**

1. Predict the prior estimate  $\tilde{x}^{aug}(t_k)$  based on Equation (8);
2. Predict the prior estimate covariance  $\tilde{P}^{aug}(t_k)$  based on Equation (9);

**Step 2 : Update**

1. Obtain the Kalman gain  $K^{aug}(t_k)$  based on Equation (5);
  2. Update posterior state estimate  $\hat{x}^{aug}(t_k)$  based on Equation (6);
  3. Update posterior state estimate covariance  $\hat{P}^{aug}(t_k)$  based on Equation (7);
- 

Fig. 3. Algorithm 2 for the PENS.

In this section, we define the estimation scenarios based on whether the shaft power information from the starter/generator is available or not. Subsequently, we present detailed algorithms for obtaining the posterior estimates and their corresponding covariance under these two scenarios, namely, the PES and PENS.

## V. IMPACT OF SHAFT POWER INFORMATION FROM THE STARTER/GENERATOR ON THE GAS GENERATOR FAULT ESTIMATION ACCURACY

This section evaluates the impact of shaft power information from the starter/generator on estimation accuracy through a comparison between PES and PENS. To facilitate this comparison, we develop MPES (Modified Posterior Estimates with Shaft power information), a modified version of PES, and demonstrate its equivalence to PENS. This equivalence enables us to use MPES as a bridge for effectively comparing PES and PENS. The results demonstrate that incorporating shaft power information significantly improves the estimation precision of each gas generator state and health parameter. This improvement becomes more pronounced under two conditions: when using a more accurate state transition model or when estimating a larger number of health parameters.

### A. Modified Posterior Estimates with Shaft Power Information (MPES) and Its Equivalence with PENS

After substituting equation (9) for equation (4) in the PES, we derive a modified estimate that is referred to as the MPES, and its algorithm is outlined as the Algorithm 3.

---

**Algorithm 3:** Modified posterior estimates with Shaft Power Information (MPES)

---

**Input :** Engine augmented state space matrix:  
 $A^{aug}(t_{k-1}), B^{aug}(t_{k-1}), C^{aug}(t_k), D^{aug}(t_k), F^{aug}(t_{k-1});$   
 Posterior state estimate and covariance at  $t_{k-1}$ :  
 $\hat{x}^{aug}(t_{k-1}), \hat{P}^{aug}(t_{k-1});$   
 Shaft power estimate from starter/generator:  
 $Pe(t_k);$

**Output:** Posterior state estimate and covariance at  $t_k$ :  
 $\hat{x}^{aug}(t_k), \hat{P}^{aug}(t_k);$

**Step 1 : Predict**

1. Predict the prior estimate  $\tilde{x}^{aug}(t_k)$  based on Equation (3);
2. Predict the prior estimate covariance  $\tilde{P}^{aug}(t_k)$  based on Equation (9);

**Step 2 : Update**

1. Obtain the Kalman gain  $K^{aug}(t_k)$  based on Equation (5);
  2. Update posterior state estimate  $\hat{x}^{aug}(t_k)$  based on Equation (6);
  3. Update posterior state estimate covariance  $\hat{P}^{aug}(t_k)$  based on Equation (7);
- 

Fig. 4. Algorithm 3 for the MPES.

The substitution that is outlined in the Algorithm 3 reveals that the MPES is derived by leveraging the precise estimate from the starter/generator, without utilizing the corresponding covariance. Instead, the pre-set large value  $P^{PeT}$ , used in the Algorithm 2 for computing the PENS, is employed as the covariance. Consequently, the MPES represents estimates that are obtained by utilizing the accurate shaft power estimates from the starter/generator, albeit with minimal belief. Following this, we now introduce the Theorem 1 to elucidate the equivalence between the MPES and PENS schemes.

**Theorem 1:** The estimation covariance and the Kalman gain in the Algorithm 3 for achieving the MPES is equal to that in the Algorithm 2 for achieving the PENS at each time step following  $t_0$ , as denoted by  $\hat{P}^{aug,MPES}(t_k) = \hat{P}^{aug,PENS}(t_k)$ ,  $K^{aug,MPES}(t_k) = K^{aug,PENS}(t_k)$  where superscript *MPES* and

> REPLACE THIS LINE WITH YOUR MANUSCRIPT ID NUMBER (DOUBLE-CLICK HERE TO EDIT) <

PENS correspond to estimates and covariance of the MPES and PENS, respectively.

**Proof:** Since both algorithms for the PENS and MPES use equations (4), (5) and (7), respectively to compute the prior covariance  $\tilde{P}^{aug,PENS}(t_k)$ ,  $\tilde{P}^{aug,MPES}(t_k)$ , the Kalman gain  $K^{aug,PENS}(t_k)$ ,  $K^{aug,MPES}(t_k)$  and the posterior covariance  $\hat{P}^{aug,PENS}(t_k)$ ,  $\hat{P}^{aug,MPES}(t_k)$ , it follows that  $\tilde{P}^{aug,PENS}(t_k) = \tilde{P}^{aug,MPES}(t_k)$ ,  $K^{aug,PENS}(t_k) = K^{aug,MPES}(t_k)$  and  $\hat{P}^{aug,PENS}(t_k) = \hat{P}^{aug,MPES}(t_k)$  when  $\hat{P}^{aug,PENS}(t_{k-1}) = \hat{P}^{aug,MPES}(t_{k-1})$ , provided that the system parameters and health parameters, as well as the measurements and inputs are the same.

Thus, it can be inferred through recursive reasoning that  $\hat{P}^{aug,MPES}(t_k) = \hat{P}^{aug,PENS}(t_k)$  and  $K^{aug,MPES}(t_k) = K^{aug,PENS}(t_k)$  at each time step following  $t_0$  when the system parameters, the initial Gaussian distribution of the system states and health parameters, as well as the measurements and inputs are the same. This completes the proof of the theorem. ■

Here, we have demonstrated the equality of the covariance and the Kalman gain between the PENS and MPES. Next, we will demonstrate that the estimates of the PENS and MPES are also the same under the conditions.

**Theorem 2:** Assuming that  $P_{[i,i]}^{aug,PENS}(t_k)$  is bounded for any  $i$  when  $P^{PeT} \rightarrow +\infty$ , where  $i$  represents any row of the matrix and the subscript  $[:,i]$  refers to the matrix element at the corresponding row and column, then it follows that as  $P^{PeT} \rightarrow +\infty$ , the difference between  $\hat{x}^{aug,PENS}(t_k)$  and  $\hat{x}^{gt-aug,MPES}(t_k)$  converges to zero following the initial time  $t_0$ .

**Proof:** By expanding equations (4) and (7), one can express the posterior estimate variance of the PENS, as follows:

$$\begin{aligned} & \hat{P}^{aug,PENS}(t_k) \\ &= (I - K^{aug,PENS}(t_k)C^{aug}(t_k))F^{aug}(t_k)P^{PeT}(t_k)F^{aug}(t_k)^T \\ & \quad (I - K^{aug,PENS}(t_k)C^{aug}(t_k))^T + (I - K^{aug,PENS}(t_k)C^{aug}(t_k)) \\ & \quad (A^{aug}(t_k)\hat{P}^{aug,PENS}(t_{k-1})A^{aug}(t_k)^T + Q^{aug}(t_k)) \\ & \quad (I - K^{aug,PENS}(t_k)C^{aug}(t_k))^T + K^{aug,PENS}(t_k)R(t_k)K^{aug,PENS}(t_k)^T \end{aligned} \quad (10)$$

It follows that all the three parts in equation (10) are positive semi-definite matrices. Considering that when  $\hat{P}_{[i,i]}^{aug,PENS}$  is bounded for any  $i$ , it follows that  $(I - K^{aug,PENS}(t_k)C^{aug}(t_k))F^{aug}(t_k) \rightarrow 0$  as  $P^{PeT} \rightarrow +\infty$ .

Using equation (6) and Theorem 1 above, and considering the same inputs and measurements, one can derive:

$$\begin{aligned} & \hat{x}^{aug,PENS}(t_k) - \hat{x}^{aug,MPES}(t_k) \\ &= (I - K^{aug,PENS}(t_k)C^{aug}(t_k))A^{aug}(t_k) \\ & \quad (\hat{x}^{aug,PENS}(t_{k-1}) - \hat{x}^{aug,MPES}(t_{k-1})) \\ & \quad + (I - K^{aug,PENS}(t_k)C^{aug}(t_k))F^{aug}(t_k)(PeT(t_k) - Pe(t_k)) \end{aligned} \quad (11)$$

Based on the result that  $(I - K^{aug,PENS}(t_k)C^{aug}(t_k))F^{aug}(t_k) \rightarrow 0$  as  $P^{PeT} \rightarrow +\infty$ , it can be inferred that if  $\hat{x}^{aug,PENS}(t_{k-1}) - \hat{x}^{aug,MPES}(t_{k-1}) \rightarrow 0$ , thus  $\hat{x}^{aug,PENS}(t_k) - \hat{x}^{aug,MPES}(t_k) \rightarrow 0$  as  $P^{PeT} \rightarrow +\infty$ .

Then through recursive reasoning, one can derive that as  $P^{PeT} \rightarrow +\infty$ ,  $\hat{x}^{aug,PENS}(t_k) - \hat{x}^{aug,MPES}(t_k) \rightarrow 0$  for each time step following the initial time  $t_0$ , under the assumptions of the theorem. This completes the proof of the theorem. ■

Theorem 2 implies the practical equivalence of estimates between the PENS and MPES. This is due to the fact that the  $P^{PeT}$  is a large number, as previously described, and when PENS is effective (signifying that the estimation error is not significantly large, i.e.,  $P_{[i,i]}^{aug,PENS}(t_k)$  is not a large value for any  $i$ ), then  $\hat{x}^{aug,PENS}(t_k)$  and  $\hat{x}^{aug,MPES}(t_k)$  are almost the same.

By combining the covariance equivalence that is presented in Theorem 2 with the equivalence of estimates that is outlined in Theorem 3, one can conclusively establish the equivalence between the PENS and the MPES.

In this subsection, we proposed the MPES and demonstrated the equivalence of the PENS and MPES. Subsequently, we will assess and compare the estimation accuracy of the PENS and PES by examining the accuracy between the MPES and PES.

### B. Comparative Estimation Accuracy Analysis of PENS & PES

In this section, we will demonstrate and derive the differences in accuracy between the PES and PENS. Given the demonstrated equivalence between the PENS and MPES in the previous subsection, we can assess the estimation accuracy of the PES relative to the PENS through a comparison with MPES.

**Theorem 3:** Assuming that the shaft power estimates and corresponding covariances from starter/generator, which are provided to the PES, are consistent with the actual system and  $P^{PeT}(t_k) > P^{Pe}(t_k)$  in each time step, then it follows that  $\varepsilon_i^{aug,MPES}(t_k) \geq \varepsilon_i^{aug,PES}(t_k)$  for any  $i$  and time step following  $t_0$ ,

where  $\varepsilon_i^{aug,MPES} = E\left[(\hat{x}_i^{aug,MPES} - x_i^{aug})^2\right]$ ,

$\varepsilon_i^{aug,PES} = E\left[(\hat{x}_i^{aug,PES} - x_i^{aug})^2\right]$ , representing the expected squared estimation errors for the  $i$ th estimate of the MPES and PES, respectively.

**Proof:** We first denote  $P_\varepsilon^{aug,MPES}(t_k)$  and  $P_\varepsilon^{aug,PES}(t_k)$  as the covariance of estimation error (CEE) [33] of the MPES and PES as follows:

$$P_\varepsilon^{aug,MPES}(t_k) = E\left[(\hat{x}^{aug,MPES} - x^{aug})(\hat{x}^{aug,MPES} - x^{aug})^T\right] \quad (12)$$

$$P_\varepsilon^{aug,PES}(t_k) = E\left[(\hat{x}^{aug,PES} - x^{aug})(\hat{x}^{aug,PES} - x^{aug})^T\right] \quad (13)$$

where subscript  $\varepsilon$  denotes the expected squared estimation error matrix.

The proof can now be transformed into demonstrating that  $P_{\varepsilon,[i,i]}^{aug,MPES}(t_k) \geq P_{\varepsilon,[i,i]}^{aug,PES}(t_k)$  for any given  $i$  and time step subsequent to  $t_0$ , under the stipulated assumptions.

Given that the parameters that are provided to compute the PES are all consistent with the actual system, it follows that the

> REPLACE THIS LINE WITH YOUR MANUSCRIPT ID NUMBER (DOUBLE-CLICK HERE TO EDIT) <

posterior covariance of the PES is equal to its CEE, namely  $P_{\varepsilon}^{aug,PES}(t_k) = \hat{P}_{\varepsilon}^{aug,PES}(t_k)$  holds for any time step following  $t_0$ . Consequently, based on equation (7), the CEE of the PES, as denoted by  $P_{\varepsilon}^{aug,PES}(t_k)$ , can be expressed as follows [33]:

$$\begin{aligned} P_{\varepsilon}^{aug,PES}(t_k) &= \hat{P}_{\varepsilon}^{aug,PES}(t_k) \\ &= (I - K^{aug,PES}(t_k)C^{aug}(t_k))\tilde{P}_{\varepsilon}^{aug,PES}(t_k) \\ &\quad \left( (I - K^{aug,PES}(t_k)C^{aug}(t_k))^T + K^{aug,PES}(t_k)R(t_k)K^{aug,PES}(t_k)^T \right) \quad (14) \\ &= (I - K^{aug,PES}(t_k)C^{aug}(t_k))\tilde{P}_{\varepsilon}^{aug,PES}(t_k) \\ &\quad \left( (I - K^{aug,PES}(t_k)C^{aug}(t_k))^T + K^{aug,PES}(t_k)R(t_k)K^{aug,PES}(t_k)^T \right) \end{aligned}$$

where

$$\begin{aligned} \tilde{P}_{\varepsilon}^{aug,PES}(t_k) &= A^{aug}(t_k)P_{\varepsilon}^{aug,PES}(t_{k-1})(t_{k-1})A^{aug}(t_k)^T \\ &\quad + F^{aug}(t_k)P^{Pe}(t_k)F^{aug}(t_k)^T + Q^{aug}(t_k) \end{aligned}$$

Due to the lack of actual shaft power distribution information in the calculations for the MPES, the posterior estimate of the MPES is not the CEE of the MPES. The CEE of the MPES is presented as follows [34],

$$\begin{aligned} P_{\varepsilon}^{aug,MPES}(t_k) &= (I - K^{aug,MPES}(t_k)C^{aug}(t_k))\tilde{P}_{\varepsilon}^{aug,MPES}(t_k) \\ &\quad \left( (I - K^{aug,MPES}(t_k)C^{aug}(t_k))^T \right. \\ &\quad \left. + K^{aug,MPES}(t_k)R(t_k)K^{aug,MPES}(t_k)^T \right) \quad (15) \end{aligned}$$

where

$$\begin{aligned} \tilde{P}_{\varepsilon}^{aug,MPES}(t_k) &= A^{aug}(t_k)\tilde{P}_{\varepsilon}^{aug,MPES}(t_{k-1})A^{aug}(t_k)^T \\ &\quad + F^{aug}(t_k)P^{Pe}(t_k)F^{aug}(t_k)^T + Q^{aug}(t_k) \end{aligned}$$

By utilizing equations (14) and (15), the expression for  $P_{\varepsilon}^{aug,MPES}(t_k) - P_{\varepsilon}^{aug,PES}(t_k)$  can be derived as shown in equation (16), as follows:

$$\begin{aligned} &P_{\varepsilon}^{aug,MPES}(t_k) - P_{\varepsilon}^{aug,PES}(t_k) \\ &= (K^{aug,MPES}(t_k) - K^{aug,PES}(t_k)) \\ &\quad \left( C^{aug}(t_k)\tilde{P}_{\varepsilon}^{aug,PES}(t_k)C^{aug}(t_k)^T + R^{gt}(t_k) \right) \\ &\quad \left( K^{aug,MPES}(t_k) - K^{aug,PES}(t_k) \right)^T \quad (16) \\ &\quad + (I - K^{aug,MPES}(t_k)C^{aug}(t_k)) \left( \tilde{P}_{\varepsilon}^{aug,MPES}(t_k) - \tilde{P}_{\varepsilon}^{aug,PES}(t_k) \right) \\ &\quad \left( I - K^{aug,MPES}(t_k)C^{aug}(t_k) \right)^T \end{aligned}$$

From equation (16), it can be observed that when  $\tilde{P}_{\varepsilon}^{aug,MPES}(t_k) \geq \tilde{P}_{\varepsilon}^{aug,PES}(t_k)$ , the right hand side of equation (16) consists of two positive semi-definite matrices, resulting in  $P_{\varepsilon}^{aug,MPES}(t_k) \geq P_{\varepsilon}^{aug,PES}(t_k)$ , where  $A \geq B$  represents that  $A - B$  is a positive semi-definite matrix. Because we have

$$\begin{aligned} &\tilde{P}_{\varepsilon}^{aug,MPES}(t_k) - \tilde{P}_{\varepsilon}^{aug,PES}(t_k) \\ &= A^{aug}(t_k) \left( P_{\varepsilon}^{aug,MPES}(t_{k-1}) - P_{\varepsilon}^{aug,PES}(t_{k-1}) \right) A^{aug}(t_k)^T \quad (17) \\ &\quad + F^{aug}(t_k) \left( P^{PeT}(t_k) - P^{Pe}(t_k) \right) F^{aug}(t_k)^T \end{aligned}$$

Therefore, through the application of recursive reasoning, it can be concluded that, given  $P^{PeT}(t_k) \geq P^{Pe}(t_k)$  and the same actual initial distribution implying  $P_{\varepsilon}^{aug,MPES}(t_0) = P_{\varepsilon}^{aug,PES}(t_0)$ ,

along with other assumptions outlined in the theorem, the inequality  $\tilde{P}_{\varepsilon}^{aug,MPES}(t_k) \geq \tilde{P}_{\varepsilon}^{aug,PES}(t_k)$  is maintained at any time step following  $t_0$ . Hence based on equation (16), one can derive that  $P_{\varepsilon}^{aug,MPES}(t_k) \geq P_{\varepsilon}^{aug,PES}(t_k)$  holds under the same conditions.

Based on the properties of positive semi-definite matrices and the definition of the CEE, one can conclude that  $\varepsilon_i^{aug,MPES} \geq \varepsilon_i^{aug,PES}$  for any index  $i$  and for all time steps subsequent to  $t_0$ , given the assumptions that are specified in the theorem. This completes the proof of the theorem. ■

We next explore the conditions under which equality is consistently achieved in the inequality  $\varepsilon_i^{aug,MPES} \geq \varepsilon_i^{aug,PES}$ . From equation (16), it follows that for the inequality  $\varepsilon_i^{aug,MPES} \geq \varepsilon_i^{aug,PES}$  to consistently hold, the  $i$ th row of the matrix  $K^{aug,MPES}(t_k) - K^{aug,PES}(t_k)$  must be zero. Referring to equation (5), it is observed that if the matrices  $F$  and  $C$  do not contain any rows entirely composed of zero elements, and matrix  $G$  does not have any columns entirely composed of zero elements, then the matrix  $K^{aug,MPES}(t_k) - K^{aug,PES}(t_k)$  will not have any rows consisting solely of zero elements. Therefore, by combining the equivalence between the PENS and MPES as demonstrated in the Theorems 1 and 2, we can conclude that  $\varepsilon_i^{aug,PENS} > \varepsilon_i^{aug,PES}$  for any  $i$  under the given estimation scenarios.

Building on the conclusion and the definitions provided in Section IV for Scenarios 1 and 2, as well as for the PES and PENS, we demonstrate that the use of shaft power information from the starter/generator can improve the accuracy of estimating each system state and health parameter. This improvement will consequently enhance the achievable FDI capabilities.

From the proof of the Theorems 1-3, it can be observed that the improvement in the estimation accuracy for each state and health parameter, due to the shaft power information, is attributable to the intrinsic characteristics of the all-electric APU gas generator. The influence of the shaft power on each state enhances the estimation of each system state. The fact that each measurement is influenced by at least one state, and in turn, each health parameter can affect at least one measurement, improves the estimation of each health parameter.

Additionally, the proof of the Theorems 1-3 reveals that the capability of shaft power estimates from the starter/generator to enhance estimation accuracy lies in providing more accurate prior estimates. This improvement becomes more pronounced with the enhancement of the accuracy of the model state transition representation. On the other hand, as the number of health parameters increases, the uncertainty and difficulty of the estimation also increases, thereby elevating the importance of accurate prior estimates. This amplifies the advantages of estimates that utilize the shaft power information.

Consequently, as the accuracy of the state transition representation or the number of health parameters in the gas generator model increases, the significance of the improvement in the estimation accuracy of system states and health parameters, enabled by the shaft power information from the

> REPLACE THIS LINE WITH YOUR MANUSCRIPT ID NUMBER (DOUBLE-CLICK HERE TO EDIT) <

starter/generator, becomes more pronounced. A detailed demonstration of this is provided in Section VI.

In this section, we have demonstrated that incorporating shaft power estimates from the starter/generator can improve the estimation accuracy of each state and health parameter of the gas generator, thereby enhancing the achievable FDI performance. We also analyzed the relationship between this improvement and the unique characteristics of the all-electric APU. Additionally, we examined the aspects that can influence the degree of achievable performance improvement. The subsequent section presents simulation results to further substantiate and demonstrate our proposed methodology.

## VI. SIMULATION RESULTS

In this section, we utilize Monte Carlo simulations to demonstrate the impact of shaft power estimates from starter/generator on FDI performance of an all-electric APU gas generator. Furthermore, we investigate the correlation between this impact, model accuracy, and number of health parameters.

First, we introduce the model of the gas generator that is used in our study. Subsequently, we present and compare the confusion matrices for the FDI in scenarios both with and without shaft power estimates derived from the starter/generator. These comparisons support our conclusion that incorporation of shaft power information significantly enhances the achievable FDI performance of gas generators.

We also present comparison results for the FDI after adjusting the noise level in the gas generator model and the number of health parameters to be estimated. The results indicate that improvements in the FDI performance are more pronounced by utilizing a more accurate model or a greater number of health parameters.

The gas generator model employed is governed by:

$$\begin{aligned} & x^{gt}(t_{k+1}) - x_{ss}^{gt}(t_k) \\ &= A^{gt}(t_k)(x^{gt}(t_k) - x_{ss}^{gt}(t_k)) + B^{gt}(t_k)(u^{gt}(t_k) - u_{ss}^{gt}(t_k)) \\ &+ E^{gt}(t_k)(\theta^{gt}(t_k) - \theta_{ss}^{gt}(t_k)) + F^{gt}(t_k)(Pe^{gt}(t_k) - Pe_{ss}^{gt}(t_k)) \end{aligned} \quad (18)$$

$$\begin{aligned} & + w^{gt}(t_k) \\ & y^{gt}(t_k) - y_{ss}^{gt}(t_k) \\ &= C^{gt}(t_k)(x^{gt}(t_k) - x_{ss}^{gt}(t_k)) + D^{gt}(t_k)(u^{gt}(t_k) - u_{ss}^{gt}(t_k)) \quad (19) \\ & + G^{gt}(t_k)(\theta^{gt}(t_k) - \theta_{ss}^{gt}(t_k)) + v^{gt}(t_k) \end{aligned}$$

where

$$\begin{aligned} & x^{gt} = N, \quad \theta^{gt} = [e^c, f^c, e^t, f^t]^T, \quad y^{gt} = [N_m, T_{3m}, P_{3m}, T_{5m}]^T, \\ & A^{gt} = 0.9962, \quad B^{gt} = 4.735 \times 10^3 \\ & C^{gt} = [1.000 \quad 0.01057 \quad 0.03051 \quad -0.005151]^T, \\ & D^{gt} = [0 \quad 2.553 \times 10^3 \quad 7.786 \times 10^3 \quad 8.444 \times 10^3]^T, \\ & E^{gt} = [187.7 \quad 370.4 \quad -57.70 \quad -24.16]^T, \quad F^{gt} = -0.2898, \\ & G^{gt} = \begin{bmatrix} 0 & 0 & 0 & 0 \\ -368.3 & 238.7 & 174.0 & -176.7 \\ -173.2 & 164.0 & 1.025 \times 10^3 & -1.299 \times 10^3 \\ -238.3 & -443.7 & -341.0 & 38.79 \end{bmatrix}, \end{aligned}$$

subscript  $ss$  represents the reference steady-state value,  $N$  represents the rotor speed (single shaft),  $N_m$  represents the measured rotor speed,  $T_{3m}$  represents the measured compressor outlet temperature,  $P_{3m}$  represents the measured compressor outlet pressure,  $T_{5m}$  represents the measured turbine outlet temperature and  $e^c, f^c, e^t, f^t$ , respectively, represent the degradation of compressor efficiency, compressor flow capability, turbine efficiency and turbine flow capability.

The above model is derived by linearizing a single-shaft turboshaft model established with GasTurb [35-37]. To maintain the shaft speed at its nominal value, a proportional-integral (PI) controller was also designed and incorporated.

The health parameters  $e^c, f^c, e^t, f^t$  represent the efficiency and flow factors of the compressor and turbine, respectively, as defined in equation (20) and (21). In a healthy state, these parameters have a baseline value of 1. Deviations from this baseline can indicate changes in efficiency and flow due to gas-path degradation. The gas-path degradation of compressors and turbines is primarily caused by issues such as blade corrosion, erosion, fouling, tip wear, etc., which lead to alterations in blade parameters and overall performance. Typically, compressor degradation results in decreased efficiency and reduced flow, whereas turbine degradation is characterized by decreased efficiency but increased flow[38-42].

$$e^c = \eta^c / \eta^{c-n}, \quad e^t = \eta^t / \eta^{t-n} \quad (20)$$

$$f^c = m^c / m^{c-n}, \quad f^t = m^t / m^{t-n} \quad (21)$$

where  $\eta^c, \eta^t$  denote the actual efficiencies of the compressor and turbine, respectively,  $\eta^{c-n}, \eta^{t-n}$  represent their nominal efficiencies,  $m^c, m^t$  indicate the actual flow rates, and  $m^{c-n}, m^{t-n}$  correspond to the nominal flow rates.

Based on the values of these health parameters, degradation is categorized into four distinct health conditions, namely: healthy, minor fault, medium fault, and severe fault. These conditions are detailed in TABLE I.

TABLE I  
HEALTH CONDITION CLASSIFICATION

	Healthy	Minor Fault	Medium Fault	Severe Fault
$e^c / f^c / e^t / f^t$	0.98-1	0.96-0.98	0.94-0.96	0.92-0.94
Sample Size	100	100	100	100

**Case 1:** We set measurement noise  $v^{gt}$  and process noise  $w^{gt}$  to be 0.5% of reference steady-state values of states and measurements, respectively. We conducted 100 Monte Carlo simulation runs for each condition as shown in TABLE I. Each simulation began completely healthy, namely all health parameters are set to 1, and gradually degrade to the target condition. We use PES and PENS algorithms as described in Section IV to estimate health parameters. Subsequently, we performed FDI scheme based on these estimation results to identify the health condition associated with each degradation. Fig. 5 illustrates the dynamic estimation results from a representative simulation sample. TABLE II shows the estimation accuracy of the PES and PENS. TABLE III-IV present FDI confusion matrices based on PES and PENS for  $e^c$

> REPLACE THIS LINE WITH YOUR MANUSCRIPT ID NUMBER (DOUBLE-CLICK HERE TO EDIT) <

and  $f^c$ , respectively. The results for  $e^t$  and  $f^t$  are similar and are therefore omitted to conserve space.

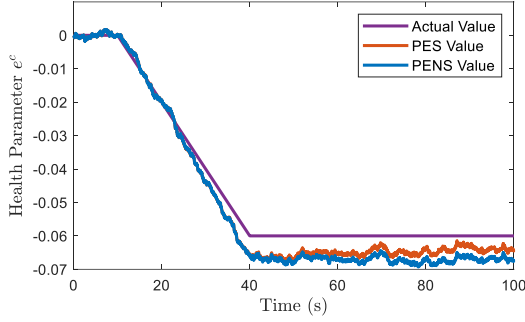


Fig. 5. Case 1 dynamic estimation results for PES and PENS

Fig.5 and TABLE II demonstrates that the PES significantly outperforms the PENS in terms of estimation accuracy for each state and health parameter. And from TABLE III-IV, we can observe that the FDI by utilizing PES demonstrate a superior performance as compared to the FDI based on the PENS particularly as fault severity escalates.

TABLE II

COMPARISON OF ACCURACY BETWEEN THE PES AND PENS UNDER CASE 1

	RMS of PES	RMSE of PENS	Accuracy Improvement of the PES over PENS
$N_L$	105.8	121.8	13.13%
$e^c$	$2.417 \times 10^{-3}$	$3.207 \times 10^{-3}$	24.63%
$f^c$	$8.749 \times 10^{-3}$	$1.194 \times 10^{-3}$	26.74%
$e^t$	$5.042 \times 10^{-3}$	$6.835 \times 10^{-3}$	26.23%
$f^t$	$6.604 \times 10^{-3}$	$9.006 \times 10^{-3}$	26.67%

TABLE III

CONFUSION MATRIX FOR  $e^c$  BASED ON THE PES/PENS UNDER CASE 1

		Estimated Class			
		Healthy	Minor Fault	Medium Fault	Severe Fault
Actual Class	Healthy	1/1	0/0	0/0	0/0
	Minor Fault	0.06/0.08	0.93/0.92	0.01/0	0/0
	Medium Fault	0/0	0.09/0.13	0.91/0.87	0/0
	Severe Fault	0/0	0/0	0.13/0.21	0.87/0.79

TABLE IV

CONFUSION MATRIX FOR  $f^c$  BASED ON THE PES/PENS UNDER CASE 1

		Estimated Class			
		Healthy	Minor Fault	Medium Fault	Severe Fault
Actual Class	Healthy	0.96/0.97	0.04/0.03	0/0	0/0
	Minor Fault	0/0	0.74/0.58	0.26/0.42	0/0
	Medium Fault	0/0	0/0	0.53/0.13	0.47/0.87
	Severe Fault	0/0	0/0	0/0	1/1

For the healthy condition, the FDI based on both the PES and PENS demonstrates comparable performance. This can be attributed to the fact that a completely healthy system does not exhibit any dynamic changes in health parameters due to degradation. Each parameter consistently maintains a value of 1, thereby reducing the complexity of the estimation, and resulting in similar FDI performance.

However, for minor, medium and severe fault conditions, the FDI systems that utilize PES exhibit markedly superior performance as compared to those using PENS. This superiority is evidenced by higher detection rates, lower false positive and negative rates, particularly in the context of higher severe faults.

Consequently, the simulation results from Case 1

substantiate the conclusion in Section V that the shaft power information can improve the estimation accuracy of each state and health parameter, resulting in an enhancement in the performance of the FDI scheme.

**Case 2:** We now reduced the process noise  $w^{st}$  to 0.1% of the reference steady-state values of the system states, while keeping all other parameters the same as in Case 1. Subsequently, we also conducted 100 Monte Carlo simulation runs for each condition as shown in TABLE I. Fig. 6 illustrates the dynamic estimation results from a representative simulation sample. The estimation accuracy of PES and PENS, along with corresponding partial FDI results are provided in TABLE V-VII.

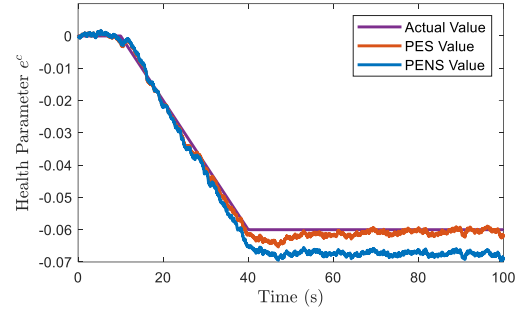


Fig. 6. Case 2 dynamic estimation results PES and PENS

Fig. 6 and TABLE V demonstrates the estimation accuracy and FDI capabilities in scenarios both with and without access to the shaft power information, given a more accurate model. Comparing TABLE V with TABLE II shows that the accuracy of the PES increases with the use of a more accurate model, while the accuracy of the PENS remains nearly unchanged under the same conditions. This leads to a larger accuracy advantage for the PES over the PENS. It can be inferred that increased accuracy in the model state transition representation enhances the positive impact of the power shaft information on the accuracy of health parameters estimation.

Note that a more accurate state transition representation leads to a more effective utilization of power shaft information, resulting in improved prior estimations and, ultimately, enhanced overall accuracy and FDI performance. However, in scenarios lacking the shaft power information, the improvement in accuracy of the state transition representation does not significantly enhance the estimation accuracy. Without the shaft power information, state transition representation plays a limited role in estimating states and health parameters, which primarily rely on the observation equation. Consequently, simulation results for Case 2 show that a more accurate model enhances the positive impact of power shaft information on accuracy of achievable health parameters estimation results.

TABLE V

COMPARISON OF ACCURACY BETWEEN THE PES AND PENS UNDER CASE 2

	RMS of PES	RMSE of PENS	Accuracy Improvement of the PES over PENS
$N_L$	63.34	121.7	47.97%
$e^c$	$1.318 \times 10^{-3}$	$3.322 \times 10^{-3}$	60.33%
$f^c$	$3.898 \times 10^{-4}$	$1.236 \times 10^{-3}$	68.47%
$e^t$	$2.326 \times 10^{-3}$	$7.075 \times 10^{-3}$	67.13%
$f^t$	$2.978 \times 10^{-3}$	$9.328 \times 10^{-3}$	68.07%

> REPLACE THIS LINE WITH YOUR MANUSCRIPT ID NUMBER (DOUBLE-CLICK HERE TO EDIT) <

TABLE VI

CONFUSION MATRIX FOR  $e^c$  BASED ON THE PES/PENS UNDER CASE 2

		Estimated Class			
		Healthy	Minor Fault	Medium Fault	Severe Fault
Actual Class	Healthy	0.98/1	0.02/0	0/0	0/0
	Minor Fault	0.02/0.1	0.94/0.89	0.04/0.01	0/0
	Medium Fault	0/0	0/0.20	1/0.80	0/0
	Severe Fault	0/0	0/0	0.03/0.29	0.97/0.71

TABLE VII

CONFUSION MATRIX FOR  $f^c$  BASED ON THE PES UNDER CASE 2

		Estimated Class			
		Healthy	Minor Fault	Medium Fault	Severe Fault
Actual Class	Healthy	0.92/0.95	0.08/0.05	0/0	0/0
	Minor Fault	0.05/0	0.89/0.60	0.06/0.40	0/0
	Medium Fault	0/0	0.04/0	0.92/0.15	0.04/0.85
	Severe Fault	0/0	0/0	0.06/0	0.94/1

**Case 3:** We assume that degradation of compressor and turbine simultaneously occurs in terms of efficiency and flow, and there exists a known proportional relationship as given by equation (22) [41]. Given that  $k^{gt-c}, k^{gt-t}$  are known fixed values, the description of the gas generator gas path degradation can be reduced from four independent health parameters  $e^{gt-c}, f^{gt-c}, e^{gt-t}, f^{gt-t}$  to two independent variables  $e^{gt-c}, e^{gt-t}$ . Next, we set the same noise level as in the Case 2 and keep all other parameters unchanged. Subsequently, we also conducted 100 Monte Carlo simulation runs for each condition as shown in TABLE I. Fig. 7 illustrates the dynamic estimation results from a representative simulation sample. The estimation accuracy of the PES and the PENS, along with the corresponding partial FDI results, are detailed in TABLE VIII-IX. Specifically, we have

$$\begin{aligned} f^{gt-c} &= 1 - k^{gt-c}(1 - e^{gt-c}) \\ f^{gt-t} &= 1 - k^{gt-t}(1 - e^{gt-t}) \end{aligned} \quad (22)$$

where  $k^{gt-c}, k^{gt-t}$  respectively, denote the known fixed correlation coefficients between the efficiency factor and the flow factor of the compressor and turbine, respectively.

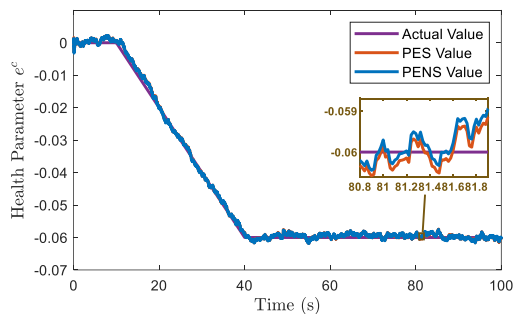


Fig. 7. Case 3 dynamic estimation results PES and PENS

Fig. 7 and TABLE VIII-IX provide estimation accuracy and FDI performance when fewer health parameters are estimated by using the same number of measurements, indicating a relatively higher sufficiency of information for estimating health parameters. In TABLE VIII, it follows that estimation accuracies of PES and PENS are nearly the same. This similarity can be attributed to the fact that estimating fewer parameters while maintaining the same number of

measurements, results in relatively less uncertainty in estimations. This diminished uncertainty arises from the assumption in Case 3 of a determined relationship among health parameters, thereby narrowing the possible distribution of parameters given same measurements. Consequently, when uncertainty is lower, contributions of shaft power estimates from starter/generator to enhancing accuracy of health parameter estimation are minimal. Furthermore, similar FDI performance based on both PES and PENS, as per TABLE IX, further supports our conclusion.

TABLE VIII

COMPARISON OF ACCURACY BETWEEN THE PES AND PENS UNDER CASE 3

	RMS of PES	RMSE of PENS	Accuracy Improvement of the PES over PENS
$N_L$	61.04	117.1	47.88%
$e^c$	$8.053 \times 10^{-4}$	$8.068 \times 10^{-4}$	0.1947%
$e^t$	$8.507 \times 10^{-4}$	$8.535 \times 10^{-3}$	0.3351%

TABLE IX

CONFUSION MATRIX FOR  $e^t$  BASED ON THE PES/PENS UNDER CASE 3

		Estimated Class			
		Healthy	Minor Fault	Medium Fault	Severe Fault
Actual Class	Healthy	0.96/0.96	0.04/0.04	0/0	0/0
	Minor Fault	0.02/0.02	0.98/0.98	0/0	0/0
	Medium Fault	0/0	0.02/0.02	0.97/0.98	0.01/0
	Severe Fault	0/0	0/0	0/0	1/1

Consequently, comparisons between Cases 3 and 2 indicate that contribution of shaft power information in improving estimation accuracy of system states and health parameters becomes more significant when more health parameters are estimated.

In the TABLE X below, we present the macro averages of accuracy, precision, recall, and F1 score for the FDI based on PES and PENS across different health conditions in Case 1, Case 2, and Case 3. From the data in TABLE X for Case 1, it is evident that PES outperforms PENS due to its use of precise shaft power information. Furthermore, the data in TABLE X for Case 2 shows that as the model accuracy improves, the advantages of PES become more pronounced. However, the data in TABLE X for Case 3 also indicates that when the number of health parameters to be estimated decreases, the importance of additional shaft power information diminishes due to reduced system uncertainty, resulting in similar performance between PES and PENS.

It is clear that the relative advantage of PES over PENS lies in its significant accuracy benefits when measurement information is relatively insufficient, the number of health parameters to be estimated is large, or the model accuracy is high. On the other hand, the relative advantage of PENS is that it does not require additional precise shaft power information provided by a generator, making it easier to deploy. It also performs well when model accuracy is not high or the number of health parameters to be estimated is small. Therefore, the choice between PES and PENS should be based on the specific scenario.

The above Monte Carlo simulations and related analyses have confirmed our conclusion that incorporating shaft power information can enhance the estimation accuracy of each state and health parameter, thereby improving the FDI performance. These improvements are especially pronounced with a more

> REPLACE THIS LINE WITH YOUR MANUSCRIPT ID NUMBER (DOUBLE-CLICK HERE TO EDIT) <

accurate model or when more health parameters are involved, as discussed in Section V.

TABLE X  
PERFORMANCE METRICS FOR FDI BASED ON PES AND PENS

		Precision	Recall	F1 Score	
Monte-Carlo Case	Case 1	PES	0.8344	0.8193	0.8162
		PENS	0.7541	0.7131	0.6927
	Case 2	PES	0.9445	0.9437	0.9438
		PENS	0.7453	0.7044	0.6850
	Case 3	PES	0.9790	0.9788	0.9788
		PENS	0.9778	0.9775	0.9775

To further validate our theoretical framework and demonstrate its practical guiding significance, we introduce a state-of-the-art hybrid deep neural network (HDNN) approach recently developed for gas generator FDI [13]. This HDNN utilizes a multi-time window convolutional bidirectional long short-term memory (CNN-BiLSTM) neural network for fault diagnosis. Following this approach, we employ two neural networks: HNS (HDNN with shaft power signal input) and HNNS (HDNN with no shaft power signal input), which are identical in architecture and hyperparameters except for the incorporation of shaft power information. Both networks are then trained and tested using consistent strategies across the aforementioned Monte Carlo simulation Cases 1-3.

The FDI performance of HNS and HNNS across Cases 1-3 is quantitatively presented through performance metrics in TABLE XI. Additionally, to provide a more intuitive visualization of the estimation differences, we plotted the dynamic estimation results of HNS and HNNS (based on HDNN method) alongside PES and PENS (based on our methods) for a sample in Case 2, as illustrated in Fig. 8. This visual comparison helps to better demonstrate the distinctions in estimation capabilities among these approaches.

TABLE XI  
PERFORMANCE METRICS FOR FDI BASED ON HNS AND HNNS

		Precision	Recall	F1 Score	
Monte-Carlo Case	Case 1	HNS	0.7153	0.6969	0.6976
		HNNS	0.6892	0.6636	0.6668
	Case 2	HNS	0.8659	0.8538	0.8546
		HNNS	0.7522	0.7246	0.7260
	Case 3	HNS	0.9455	0.9400	0.9438
		HNNS	0.9538	0.9334	0.9370

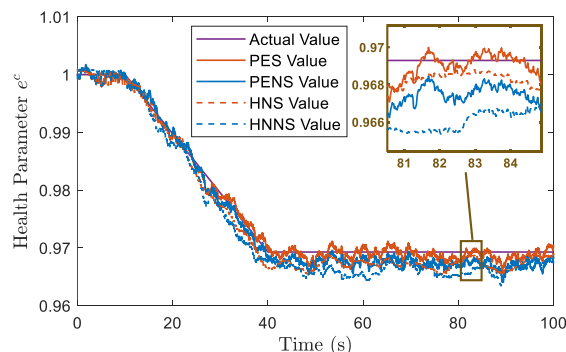


Fig. 8. Case 2 dynamic estimation results for HNS and HNNS

Through the comparison of TABLE X and TABLE XI, along with the performance shown in Fig. 8, we can observe that although HDNN, as a state-of-the-art method, performs reasonably well, particularly in Case 3 where uncertainty are relatively low and data is relatively sufficient, HNS and HNNS approaching the performance of our PES and PENS methods. However, they merely approach but cannot surpass our methods, as HNS consistently underperforms PES, and HNNS falls short of PENS. This demonstrates the superiority of our method as an optimal estimator, which even state-of-the-art approaches cannot exceed.

Furthermore, comparing TABLE X and TABLE XI, together with the results shown in Fig. 8, reveals that HNS consistently outperforms HNNS across all scenarios, with the largest advantage in Case 2 and relatively smaller margins in Cases 1 and 3. This has two significant implications. First, it validates our conclusion that incorporating shaft power information can substantially improve fault estimation and FDI, with the improvement becoming more pronounced as model accuracy increases and the number of health parameters to be estimated grows. Second, it proves that our theoretical framework has strong practical guidance value, pointing the way forward for all-electric APU FDI technology development and providing clear direction for the improvement and evolution of current methodologies.

It should be noted that PES and HNS are based on accurate shaft power information. How to obtain such information is our future work, which involves addressing the challenges of APU electrification mentioned in this paper - specifically, achieving stable estimation of high-power starter/generator's status, faults and power under various conditions, disturbances and failures.

## VII. CONCLUSION

This study presents a comprehensive analysis of the opportunities and challenges associated with FDI in the context of APU electrification. We have proposed an innovative methodology to enhance both state and fault estimation of the gas generator in an all-electric APU by leveraging generator information. Our rigorous analysis demonstrates that the incorporation of starter/generator shaft power information significantly improves the optimal estimation accuracy for both states and health parameters of the gas generator. This enhancement becomes particularly evident when employing more accurate models or when estimating an expanded set of health parameters. The effectiveness of our proposed methodology has been thoroughly validated through extensive simulation studies. Comparative analyses with state-of-the-art methods not only demonstrate the superiority of our approach but also reveal that conventional methods can achieve substantial improvements through the integration of shaft power information, aligning with our theoretical predictions. This verifies both the effectiveness and guiding significance of our theoretical framework.

Our research findings have provided a perspective on why joint fault diagnosis of the starter/generator and gas generator is necessary for all-electric APU, how to conduct such joint diagnosis, what is its effectiveness, and what factors affect its effectiveness. These offer guidance and lay the theoretical foundation for the development of current fault diagnosis

algorithms for gas generators in all-electric APU. In addition to its application in all-electric APU, our research findings can also be directly applied to future hybrid electric aircraft, including turboelectric and series hybrid electric architectures. These systems, which are based on aviation gas turbines dedicated to electrical power generation, share nearly identical principles and structures with all-electric APU. Moreover, our theoretical framework has the potential to be extended to other electro-mechanical systems with similar structures, such as REEV and wind turbines. In the future, we will further investigate the new challenges posed by the all electrification of APU as discussed in this paper. We aim to explore joint fault diagnosis algorithms for starter-generators and gas generators that are capable of simultaneously exploiting new opportunities and addressing new challenges.

#### REFERENCES

- [1] E. Sayed *et al.*, "Review of electric machines in more-/hybrid-/turbo-electric aircraft," *IEEE Trans. Transp. Electrifi.*, vol. 7, no. 4, pp. 2976-3005, 2021.
- [2] V. Madonna, P. Giangrande, and M. Galea, "Electrical power generation in aircraft: Review, challenges, and opportunities," *IEEE Trans. Transp. Electrifi.*, vol. 4, no. 3, pp. 646-659, 2018.
- [3] A. Barzkar and M. Ghassemi, "Components of electrical power systems in more and all-electric aircraft: A review," *IEEE Trans. Transp. Electrifi.*, vol. 8, no. 4, pp. 4037-4053, 2022.
- [4] B. Sarlioglu and C. T. Morris, "More electric aircraft: Review, challenges, and opportunities for commercial transport aircraft," *IEEE Trans. Transp. Electrifi.*, vol. 1, no. 1, pp. 54-64, 2015.
- [5] Y. Shen and K. Khorasani, "Hybrid multi-mode machine learning-based fault diagnosis strategies with application to aircraft gas turbine engines," *Neural Netw.*, vol. 130, pp. 126-142, 2020.
- [6] E. Naderi and K. Khorasani, "Data-driven fault detection, isolation and estimation of aircraft gas turbine engine actuator and sensors," *Mech. Syst. Signal Proc.*, vol. 100, pp. 415-438, 2018.
- [7] C. Skliros, F. Ali, and I. Jennions, "Fault simulations and diagnostics for a Boeing 747 Auxiliary Power Unit," *Expert Syst. Appl.*, vol. 184, p. 115504, 2021.
- [8] X. Liu, Z. Li, L. Wang, L. Liu, and X. Peng, "Performance parameter estimation of aircraft auxiliary power unit via a fusion model," presented at the International Conference on Sensing, Diagnostics, Prognostics, and Control (SDPC), 2019.
- [9] F. Wang, J. Sun, X. Liu, and C. Liu, "Aircraft auxiliary power unit performance assessment and remaining useful life evaluation for predictive maintenance," *Proceedings of the Institution of Mechanical Engineers, Part A: Journal of Power and Energy*, vol. 234, no. 6, pp. 804-816, 2020.
- [10] Y. Ji *et al.*, "Time-to-Failure Analysis of Short-Duty Cycle, Inverter-Fed Electrical Machines Exposed to Prevailing Electrical Stress," *IEEE Trans. Aerosp. Electron. Syst.*, vol. 59, no. 6, pp. 9368-9378, 2023.
- [11] S. Nadarajan, S. K. Panda, B. Bhangu, and A. K. Gupta, "Online model-based condition monitoring for brushless wound-field synchronous generator to detect and diagnose stator windings turn-to-turn shorts using extended Kalman filter," *IEEE Trans. Ind. Electron.*, vol. 63, no. 5, pp. 3228-3241, 2016.
- [12] J. Cui, G. Shi, and Z. Zhang, "Fault detection of aircraft generator rotating rectifier based on SAE and SVDD method," presented at the Prognostics and System Health Management Conference (PHM-Harbin), 2017.
- [13] Di ZHOU, X. Zhuang, and H. Zuo, "A hybrid deep neural network based on multi-time window convolutional bidirectional LSTM for civil aircraft APU hazard identification," *Chin. J. Aeronaut.*, vol. 35, no. 4, pp. 344-361, 2022.
- [14] U. Ahmed, F. Ali, and I. Jennions, "A review of aircraft auxiliary power unit faults, diagnostics and acoustic measurements," *Prog. Aeosp. Sci.*, vol. 124, p. 100721, 2021.
- [15] N. Jiao, Z. Li, S. Mao, C. Sun, and W. Liu, "Aircraft Brushless Wound-Rotor Synchronous Starter - Generator: A Technology Review," *IEEE Trans. Power Electron.*, vol. 38, no. 6, pp. 7558-7574, 2023.
- [16] C. Yang, M. Lu, and C. Liaw, "Development of an Aircraft Electric Power Architecture With Integrated Ground Power Unit," *IEEE Trans. Aerosp. Electron. Syst.*, vol. 58, no. 4, pp. 3446-3459, 2022.
- [17] W. Hassan, G. A. Hussain, F. Mahmood, M. Shafiq, and G. C. Montanari, "Effects of Temperature and Pressure on Failure Risk of Electric Motors Based on Partial Discharge Measurements," *IEEE Trans. Aerosp. Electron. Syst.*, vol. 59, no. 5, pp. 5624-5633, 2023.
- [18] R. Panday *et al.*, "Analyzing gas turbine-generator performance of the hybrid power system," *IEEE Trans. Power Syst.*, vol. 37, no. 1, pp. 543-550, 2021.
- [19] M. D. Bui, U. Schaefer, S. Dieckerhoff, N. P. Quang, and K. Strunz, *Maximum Torque Control of a High Speed Switched Reluctance Starter/generator Used in More/all Electric Aircraft*: Technische Universität Berlin, 2014.
- [20] J. Ye *et al.*, "A real-time model predictive controller for power control in extended-range auxiliary power unit," *IEEE Trans. Veh. Technol.*, vol. 70, no. 11, pp. 11419-11432, 2021.
- [21] X. Zhang, Z. Wu, X. Hu, W. Qian, and Z. Li, "Trajectory optimization-based auxiliary power unit control strategy for an extended range electric vehicle," *IEEE Trans. Veh. Technol.*, vol. 66, no. 12, pp. 10866-10874, 2017.
- [22] D. Liu, "Improvement of the In-Cycle Speed Fluctuation and System Efficiency of an Auxiliary Power Unit," University of Bath, 2016.
- [23] X. Gong and W. Qiao, "Imbalance Fault Detection of Direct-Drive Wind Turbines Using Generator Current Signals," *IEEE Trans. Energy Convers.*, vol. 27, no. 2, pp. 468-476, 2012.
- [24] N. Peri V S I C, P. H. Kirkegaard, and B. J. Pedersen, "Cost-effective shaft torque observer for condition monitoring of wind turbines," *Wind Energy*, vol. 18, no. 1, pp. 1-19, 2015.
- [25] S. Pang, Q. Li, and H. Feng, "A hybrid onboard adaptive model for aero-engine parameter prediction," *Aerosp. Sci. Technol.*, vol. 105, p. 105951, 2020.
- [26] B. R. Endurthi, "Linearization and health estimation of a turbofan engine," Cleveland State University, 2004.
- [27] J. Zhang, J. Fang, T. Zhang, L. Li, and X. Zhang, "Component-Level Modeling of More Electric Auxiliary Power Units for Cooperative Control," *Aerospace*, vol. 9, no. 12, p. 803, 2022.
- [28] X. Lang *et al.*, "Fault Tolerant Control of Advanced Power Generation Center for More-Electric Aircraft Applications," *IEEE Trans. Transp. Electrifi.*, vol. 8, no. 4, pp. 4173-4189, 2022.
- [29] Y. Chen, Y. Guo, X. Yan, and H. Mao, "Multiple Delay-Dependent Guaranteed Cost Control for Distributed Engine Control Systems with Aging and Deterioration," *Aerospace*, vol. 9, no. 2, p. 88, 2022.
- [30] T. Kobayashi and D. L. Simon, "Aero-Engine Real-Time Models and Their Applications," presented at the Proceedings of the ASME Turbo Expo, 2003.
- [31] J. Chen, Z. Hu, and J. Wang, "Aero-engine real-time models and their applications," *Math. Probl. Eng.*, vol. 2021, pp. 1-17, 2021.
- [32] X. Du, X. Sun, Z. Wang, and A. Dai, "A scheduling scheme of linear model predictive controllers for turbofan engines," *IEEE Access*, vol. 5, pp. 24533-24541, 2017.
- [33] D. Simon, *Optimal state estimation: Kalman, H infinity, and nonlinear approaches*: John Wiley & Sons, 2006.
- [34] T. Shao, Z. Duan, and Z. Tian, "Performance Ranking of Kalman Filter With Pre-Determined Initial State Prior," *IEEE Signal Process. Lett.*, vol. 28, pp. 902-906, 2021.
- [35] S. Zhang, Y. Guo, and J. Lu, "Research on aircraft engine component-level models based on GasTurb/MATLAB," *Journal of aerospace power*, vol. 27, no. 12, pp. 2850-2856, 2012.
- [36] H. Mao, Y. Guo, R. Li, and C. Lai, "Versatile simulation platform for turboshaft engine control system," presented at the Chinese Control Conference (CCC), 2019.
- [37] L. I. Ruichao, G. Yingqing, S. K. Nguang, and C. Yifeng, "Takagi-Sugeno fuzzy model identification for turbofan aero-engines with guaranteed stability," *Chin. J. Aeronaut.*, vol. 31, no. 6, pp. 1206-1214, 2018.
- [38] D. Simon and D. L. Simon, "Aircraft turbofan engine health estimation using constrained Kalman filtering," *J. Eng. Gas Turbines Power*, vol. 127, no. 2, pp. 323-328, 2005.
- [39] D. K. Frederick, J. A. Decastro, and J. S. Litt, "User's guide for the commercial modular aero-propulsion system simulation (C-MAPSS)," NASA, 2007.
- [40] Y. G. Li, "Gas Turbine Performance and Health Status Estimation Using Adaptive Gas Path Analysis," *Journal of Engineering for Gas Turbines and Power*, vol. 132, no. 4, 2010.
- [41] S. G. Zhang, Y. Q. Guo, and X. L. Chen, "Performance evaluation and simulation validation of fault diagnosis system for aircraft engine," *Chinese J. Propulsion Technology*, vol. 34, no. 8, pp. 1121-1127, 2013.
- [42] A. J. Volponi, "Gas Turbine Engine Health Management: Past, Present, and Future Trends," *Journal of Engineering for Gas Turbines and Power*, vol. 136, no. 5, 2014.